

# **DESIGN AND PERFORMANCE ASSESSMENT OF FLUID VISCOUS DAMPERS AND FRICTION DAMPERS FOR A SEISMICALLY EXCITED STEEL BUILDING WITH VERTICAL SETBACKS**

Ritesh Gulshan

Former Post Graduate Student, Department of Civil Engineering  
Indian Institute of Engineering Science and Technology  
Shibpur, Howrah-711103, E mail id: *gulshan.ritesh95@gmail.com*

Tanmoy Konar

Former Research Scholar, Department of Civil Engineering  
Indian Institute of Engineering Science and Technology  
Shibpur, Howrah-711103, E mail id: *3tanmoykonar@gmail.com*

Aparna Dey Ghosh (Corresponding Author)

Professor, Department of Civil Engineering  
Indian Institute of Engineering Science and Technology  
Shibpur, Howrah-711103, E mail id: *aparna@civil.iests.ac.in*

## **ABSTRACT**

The seismic performance of structures can substantially be improved by incorporating supplemental dampers. Of these, fluid viscous dampers (FVDs) and friction dampers (FDs) have gained such commercial standing that they can be accessed off the shelf as per the requirements. For a building, it would be of interest to know how the choice of a particular damper system should be made. Given this, the present study is focused on the comparison of the design and performance of these two devices. A steel building with vertical setbacks is selected for this purpose. The supplemental damping required to be provided by the dampers is determined using the Capacity Spectrum Method. The damper design includes the determination of the design characteristics of FVDs and FDs, such as the damping coefficients of FVDs and the slip loads of FDs. These design parameters are obtained based on the approach of story shear strain energy proportional distribution. Since brace stiffness affects the performance of dampers, an iterative study is conducted to obtain the optimal stiffness of the brace incorporating the dampers. Further, considering its advantage over the linear counterpart, nonlinear FVD is considered in the present study. The effectiveness of the dampers is assessed through nonlinear dynamic analyses of the uncontrolled and controlled building structure under recorded seismic excitations. Results indicate that both the acceleration and displacement responses of the building with vertical irregularity can be well-controlled with the provision of the proposed damper schemes. However, FDs achieve a larger reduction in the displacement response for strong ground motion, while FVDs are more effective in acceleration response control.

**KEYWORDS:** Aseismic Design; Capacity Spectrum Method; Fluid Viscous Damper; Friction Damper; Steel Building; Vertical Geometry Irregularity

## **INTRODUCTION**

As is well-known, the conventional practice of aseismic design permits the reduction of design forces below the elastic level on the premise that inelastic action in a suitably designed structure will provide the structure with significant energy dissipation potential and enable it to survive a severe earthquake without collapse (Moustafa, 2011; Ucar and Merter, 2019). This inelastic action is typically intended to occur in the specially detailed critical regions of the structure (Shah et al., 2016). Inelastic behavior in these regions, while able to dissipate substantial energy, also often results in significant damage to the structural member. Further, although the regions may be well-detailed, their strength and stiffness will degrade with repeated inelastic cycles (Rodgers and Mahin, 2004). This will lead to degradation of the hysteretic behavior of the regions. As a response to these inherent shortcomings of the conventional aseismic design, several approaches have been developed, such as the addition of energy absorbers to a structure (Kareem et al., 1999; Ghosh and Konar, 2023). The aim of including energy absorbers in a structure for earthquake resistance is to concentrate hysteretic behavior in specially designed and detailed regions of the

structure and to avoid inelastic behavior in primary gravity load-resisting structural elements, except perhaps under the most severe conditions (Housner et al., 1997). The fluid viscous damper (FVD) and the friction damper (FD) are two popular passive dampers that follow this mechanism to protect structures from damage during an earthquake. The chief reason for the popularity of these two dampers is the non-requirement of architectural space for installation and commercial availability.

An FVD is available in several configurations, such as the pot damper, the wall damper, and the cylindrical damper (Taylor device). The last is one of the most common and operates by forcing the fluid contained in a cylinder to flow through a restrictive control orifice during the longitudinal movement of the device (Qian et al., 2012). The fluid flows through this orifice at high speed as the damper strokes and this leads to energy dissipation. The shape of the piston head determines the damping characteristics. The FVD is a velocity-dependent damper. Though operating on the same premise as many of the other forms of energy dampers, the FVD holds several advantages. Foremost, the performance of the FVD is essentially out of phase with primary bending and shearing stresses in the structure. Thus, the device may be effectively employed to reduce the internal shear forces, bending moment, and deflections. Furthermore, by requiring little maintenance, they have become very attractive options for civil engineering applications. The pioneering work on the civil engineering application of FVD was carried out by de Silva (1981). There has been a large volume of research on FVD since then (De Domenico et al., 2019). Nowadays FVDs have become quite common in the construction of new structures and retrofits in seismic zones. About 20% of tall buildings with supplemental damping mechanisms have FVDs (Lago et al., 2018).

FDs generally are made by clamping metal plates together that can move (slip) relative to each other, leading to dry friction between the plates and subsequently dissipation of input energy (Jaisee et al., 2021). The application of FDs in civil engineering structures was pioneered by Pall et al. (1980). The FD is a displacement-dependent damper. An FD shows nearly rectangular hysteretic behavior with a stick-slip phenomenon. FDs slip at a predefined load called the slip load. In the design of an FD system, the dampers have an optimum slip load so that the dampers slip prior to yielding of the primary structure. When the slip load is much higher than the optimum value, the stick phase will be dominant without slipping, and no energy will be dissipated. On the other hand, when the slip load is considerably low, FDs will provide little supplemental damping. However,  $\pm 20\%$  variation in the slip load from the optimum value does not have a significant influence on the damper performance (Pall and Pall, 2004; Taiyari et al., 2019). This is an advantage of the FD. Further, FDs possess a high energy-dissipation capacity and a stable cyclic behavior. FDs are relatively easy and inexpensive to design, manufacture and install, and can be customized to match the dynamic properties of a structure. This leads to a large number of successful real-life installations of FDs around the globe [<https://quaketek.com/applications/>, n.d. ; <https://www.dampstech.com/japan>, n.d. ; [http://www.palldynamics.com/P1\\_usa.htm](http://www.palldynamics.com/P1_usa.htm), n.d.].

It may be inferred from the above discussion that both FVD and FD have a significant share among passive dampers in civil engineering applications. Therefore, a comparison of the efficacy of FVD and FD in improving the seismic performance of buildings has significant relevance. Here, it is pertinent to mention that most of the research on the performance assessment of FVD and FD deals with regular buildings. However, in practice, buildings often have structural irregularities, and that increases the level of seismic vulnerability of the buildings (Mouhine and Hilali, 2022). The structural irregularity may be in plan or elevation. In modern cities, vertical irregularities are common features in buildings due to serviceability, aesthetics, and other architectural requirements (Sarkar et al., 2010); Ahmed et al., 2022). Vertical irregularities in buildings mostly arise from setbacks or abrupt reductions in the lateral dimension of the building. Given this, a steel building with vertical setbacks is considered for the present study. Further, unlike most of the research carried out on FVDs and FDs, in the present study, nonlinear dynamic analysis of the controlled and uncontrolled structure is carried out to evaluate the efficacy of the damper systems. In what follows, first, the supplemental damping required to restrict the response of an example steel building with vertical setback to within the desired performance level is estimated using the Capacity Spectrum Method (CSM). Next, the design of the FVD and FD systems are illustrated. This is followed by the determination of the efficacy of the designed damper systems under recorded seismic ground motions. The performances of the dampers are compared and the salient conclusions of the study are presented.

## STEEL BUILDING WITH SETBACKS

### 1. General Description and Modelling

The considered building is a 12-story-tall steel frame, which is 44 m in elevation above the ground level with a setback at the third story, as depicted in Figure 1 (Hwang et al., 2013). The floors are 4.5 m high below the setback and 3.5 m high above the setback. The beam and column sections are given in Table 1. In addition to dead load, 3.5 kN/m<sup>2</sup> live load on floors and wall loads was considered. A live load reduction factor of 0.5 for all floors and no live load for the roof was considered while calculating the seismic weight as per IS:1893 (Part-1) (2016). The characteristic yield strength of structural steel for column and beam was taken as 345 MPa and 250 MPa respectively.

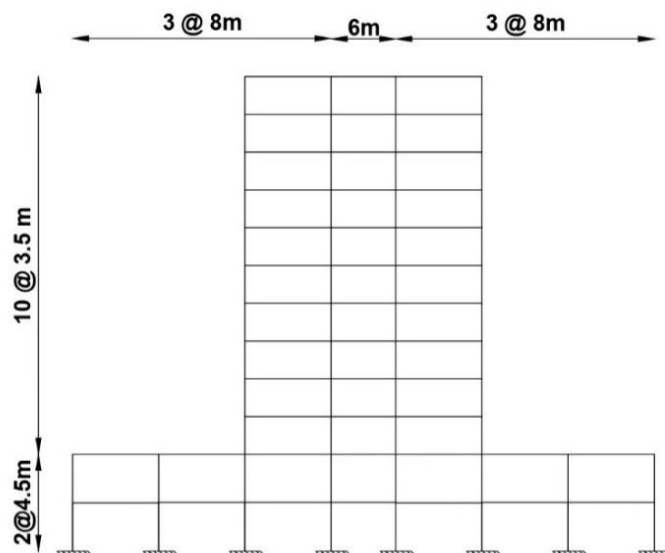


Fig. 1 Elevation of the considered steel building with setbacks

Table 1: Column and Beam Sections of the considered building

Story	Column		Beam	
	Section Type	Dimension (mm)	Section Type	Dimension (mm)
1-2	Tube	350×350×12	Wided Flange	450×225×12×24
3-5		300×300×12		350×225×12×20
6-8		250×250×10		340×225×10×16
9-12		250×250×08		330×225×10×14

The building was modeled in the SAP2000 v20 software as a two-dimensional full moment-resisting frame. A fixed-base boundary condition was considered at the column bases and the soil structure interaction effects were neglected. Floor diaphragms were assumed to be rigid in-plane, but the contribution of the floor slabs to the flexural behavior of the beams was neglected. Further, any contribution of the non-structural elements to the strength and stiffness of the structure was ignored. The inherent damping of the structure was assumed as 5% (IS:1893 (Part-1), 2016). The fundamental natural period of the building was determined as 2.79 s. Both geometric nonlinearity and material nonlinearity were included in the analysis. In order to simulate the nonlinear force-deformation behavior of the structure, hinges were assigned at the ends of each frame element, which represented the concentrated post-yield behavior in case of non-linear static and dynamic analysis. The hinge property was adopted based on the FEMA 356 (2000) guidelines, wherein the force-deformation relationship is idealized as a multi-linear curve described by points A (unstressed), B (yielding), C (ultimate capacity), D (residual resistance) and E (collapse) (Figure 2). In the force-deformation curve, BC indicates the strain-hardening phenomenon. On line BC, different acceptance limits, namely, the immediate occupancy (IO), life safety (LS), and collapse prevention (CP) are located. In the structural model, moment (M3) hinges are assigned to beam elements, while axial-moments (P-M2-M3) hinges that represent coupled axial force-moment behavior are assigned to column elements. Both hinge types are deformation controlled, that is, ductile.

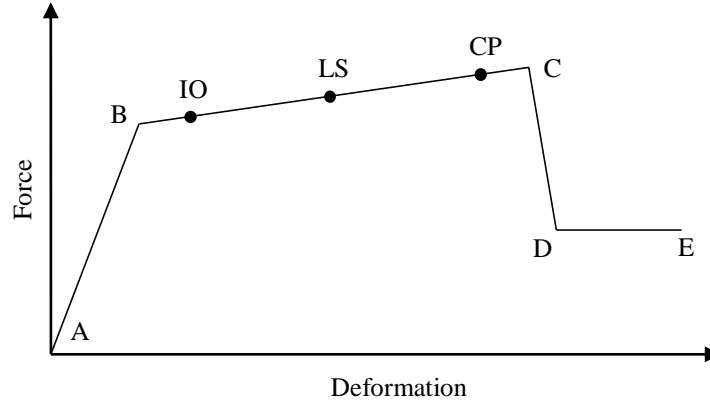


Fig. 2 Idealized force-deformation relationship as per FEMA-356 (2000)

## 2. Estimation of Required Supplemental Damping

The Capacity Spectrum Method (CSM) is used for the estimation of the supplemental damping required to be provided by the damper system (ATC 40 Vol. 1, 1996); Freeman, 2004; Ferraioli, 2016). In CSM, the capacity of a structure is characterized by a pushover curve that indicates the base shear force-roof displacement relationship derived through a nonlinear static analysis, by subjecting the structure to monotonic increasing lateral load until the structure fails. The pushover curve is then transformed into the acceleration-displacement-response-spectra or the capacity spectrum, which provides the lateral deformation-resisting capacity of the structure. In the present work, the pushover curve, as shown in Figure 3, is obtained through a displacement-controlled nonlinear static analysis carried out in SAP2000 v20. The performance levels are marked on the curve in Figure 3. Further, the assumed parameters for generating the capacity spectrum from the pushover curve are listed in Table 2 (ATC 40 Vol. 1, 1996). The shaking intensity is given by the product  $(Z \times E \times N) = 0.4$ . For soil type D and shaking intensity 0.4, seismic coefficients are obtained as  $C_a = 0.44$  and  $C_v = 0.64$  respectively from Tables 4-7 and 4-8 of ATC 40 Vol. 1 (1996). The capacity spectrum generated using SAP2000 v20 for the structure is presented in Figure 4. As expected, beyond point C (ultimate capacity), there is a sudden drop in the pushover curve as a result of significant strength degradation of the structure.

To determine the total damping ratio required for the structure equipped with a damper system, a point is required to be chosen on the capacity curve such that the structure is expected to not deform beyond this point. This point is termed the desired point. In the present study, the building is intended to perform within the elastic limit. Therefore, the desired point is chosen between A and B, and at that point, the values of spectral acceleration,  $S_a$ , and spectral displacement,  $S_d$ , are noted from the capacity spectrum (Figure 4).

**Table 2: Assumed parameters for generation of capacity spectrum (ATC 40, 1996)**

Parameters	Value
Structural behavior type	Type B (Building is new and long-duration shaking is expected during earthquake)
Zone factor ( $Z$ )	0.4 (Site is located in high seismic zone)
Near-source factor ( $N$ )	1 (Enhancement in seismic effect due to closeness of the site from earthquake source is not considered)
Earthquake level factor ( $E$ )	1 (Building is designed for design level earthquake, which has 10% probability of exceedance in 50 years period)
Soil type	Type D (Site has stiff soil (Standard penetration test values 5 - 50))

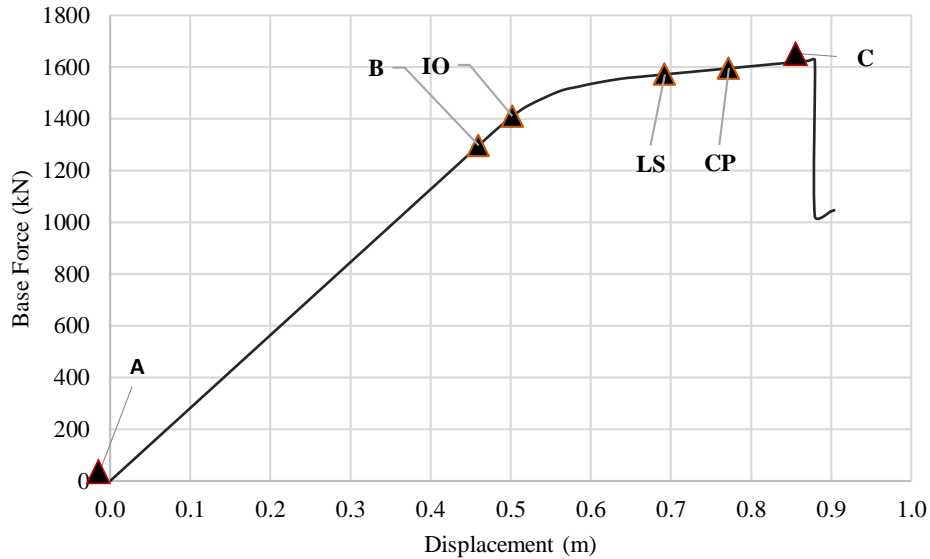


Fig. 3 Pushover curve for the considered building

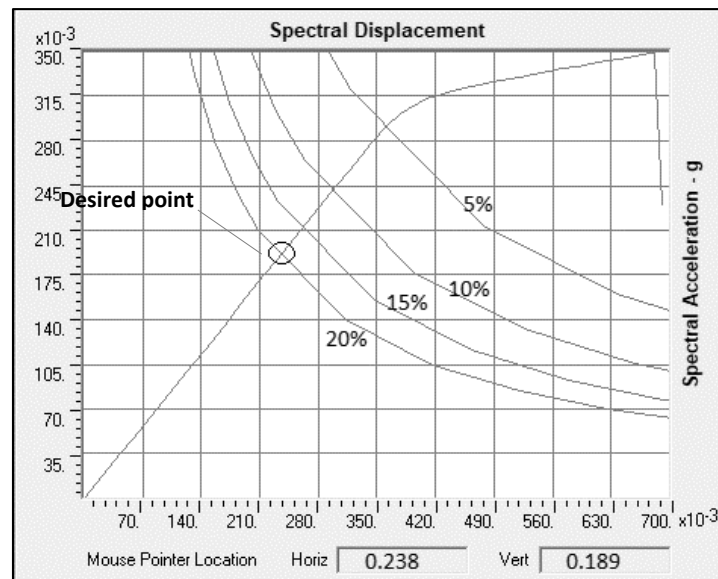


Fig. 4 Capacity spectrum for the considered building

In Figure 4, along with the capacity spectrum, a family of demand spectra with different damping ratios is also plotted. The demand spectrum that intersects the capacity spectrum at the desired point as noted above provides the total damping ratio required by the structure to perform within the desired point/performance level. Hence, in the present case, the total required damping ratio for the building is 20%. As already mentioned, the structure has an inherent damping of 5%. Thus, following a simplistic approach of adding the inherent damping of the structure to the damping ratio from the supplemental damping system to obtain the total required damping ratio of the controlled building (Hwang et al., 2013; Banazadeh et al., 2017), the required damping ratio from the supplemental damping system is 15%.

### INPUT GROUND MOTIONS

Three ground motions are considered for nonlinear dynamic analysis. The details of these ground motions, including peak ground acceleration (PGA) and Arias intensity ( $I_A$ ), are provided in Table 3. The digitized data for the input ground accelerograms is obtained from the strong motion database of the Pacific Earthquake Engineering Research Centre [PEER (n.d.)]. The ground acceleration time histories are shown in Figure 5. While choosing the ground motions, it is ensured that the fundamental natural frequency of the

building lies within the dominant frequency range of the ground motions. In this study, the ground motion Input C is considered a strong earthquake with high PGA and  $I_A$ . On the other hand, Inputs A and B are moderate earthquakes with relatively less, but still significant PGA, and  $I_A$ . The target spectrum, the spectrum of the considered ground motions, and the average spectrum are shown in Figure 6. Here, the target spectrum is as per the zone factor considered in Table 2.

**Table 3: Description of ground motions considered for nonlinear dynamic analysis**

Designation	Event	Date	Station	Component	PGA	$I_A$ (m/s)
Input A	Imperial Valley-02	5/19/1940	El Centro Array #9	180°	0.32g	1.6
Input B	Chi-Chi	9/20/1999	CHY101	90°	0.33g	3.0
Input C	Gazli	5/17/1976	Karakyr	0°	0.71g	5.7

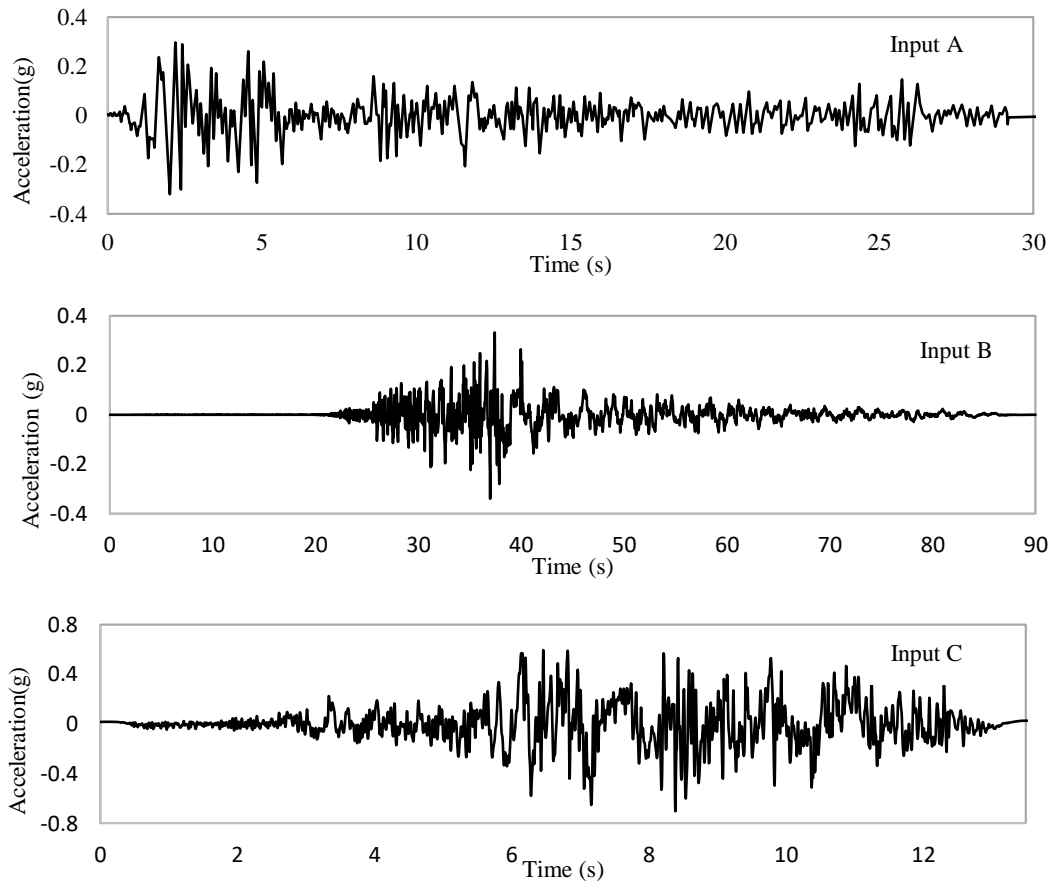


Fig. 5 Accelerogram of ground motions considered for nonlinear dynamic analysis

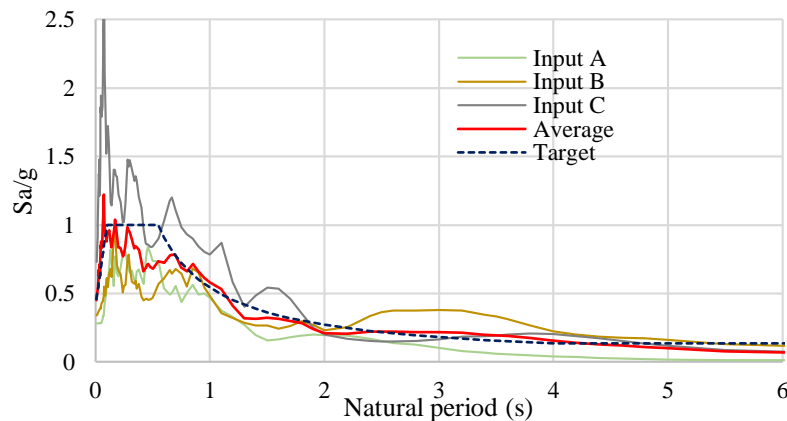


Fig. 6 Acceleration spectrum of considered scaled ground motions

## DESIGN OF DAMPER SYSTEMS

### 1. Fluid Viscous Damper (FVD) system

In this study, nonlinear FVDs are considered as it is more effective than their linear counterpart (Narkhede and Sinha, 1999). It may be noted that the viscous dampers possess no storage stiffness. Hence, their addition will not affect the story shear strain energy expressed in terms of modal strain energy. Thus, the story shear strain energy proportional distribution of dampers is expected to be effective for an irregular structure, as assigning a higher damping coefficient at the location where the story shear strain energy is larger will result in a greater contribution from the viscous dampers to the system damping ratio. While designing linear FVDs for a structure with vertical irregularity, Hwang et al. (2013) followed the same approach and distributed the damping coefficients along the height of the structure proportional to story shear strain energy. In this study, the methodology is extended to nonlinear FVDs.

The damping ratio contributed by supplemental dampers,  $\xi_d$ , is given by FEMA 356 (2000),

$$\xi_d = \frac{\sum_j E_j}{4\pi U_t} \quad (1)$$

where,  $E_j$  and  $U_t$  respectively denote the total energy dissipated by supplemental damper  $j$  in one cycle of motion and the maximum strain energy of the structure.

Further, when a structure is provided with nonlinear FVDs as supplemental dampers, the damping ratio contributed by the supplemental dampers corresponding to the first mode of vibration can be expressed as (Seleemah and Constantinou, 1997; Hanson and Soong, 2001),

$$\xi_d = \frac{T^{2-\alpha} \sum_j C_j \lambda f_j^{1+\alpha} \phi_{rj}^{1+\alpha}}{(2\pi)^{3-\alpha} A^{1-\alpha} \sum_i m_i \phi_i^2} \quad (2)$$

where,  $T$  = fundamental natural period of the structure,  $\alpha$  = damping exponent,  $C_j$  = damping coefficient of the dampers at the  $j$ th story,  $\lambda$  = a non-dimensional parameter given by Equation (3),  $f_j$  = magnification factor depending on the installation of dampers,  $\phi_{rj}$  = relative displacement between the ends of the damper  $j$  in the horizontal direction in the first mode of vibration,  $A$  = roof response amplitude,  $m_i$  = mass of the  $i$ th story, and  $\phi_i$  = normalized horizontal modal displacements of the  $i$ th story.

$$\lambda = 2^{2+\alpha} \frac{\Gamma^2 \left(1 + \frac{\alpha}{2}\right)}{\Gamma(2 + \alpha)} \quad (3)$$

Now, the damping coefficient proportional to strain energy can be expressed as

$$C_j = k S_j \phi_{rj} \quad (4)$$

where  $k$  is the proportionality constant. The total damping coefficient of the structure is then equal to

$$\sum_i C_i = k \sum_i S_i \phi_{ri} \quad (5)$$

From Equations (4) and (5), the damping coefficient at each story can be expressed as

$$C_j = \frac{S_j \phi_{rj}}{\sum_i S_i \phi_{ri}} \sum_i C_i \quad (6)$$

On substituting Equation (6) in Equation (2) and rearranging the terms, the following is obtained.

$$\sum_i C_i = \frac{(2\pi)^{3-\alpha} \xi_d A^{1-\alpha} (\sum_i m_i \phi_i^2) (\sum_i S_i)}{T^{2-\alpha} \sum_i [S_i \lambda f_i^{1+\alpha} \phi_{ri}^{1+\alpha}]} \quad (7)$$

Again, on substituting Equation (7) in Equation (6), the damping coefficient at each story can be expressed as

$$C_j = \frac{(2\pi)^{3-\alpha} \xi_d A^{1-\alpha} (S_j \phi_{rj}) (\sum_i m_i \phi_i^2) \sum_i S_i}{T^{2-\alpha} \lambda \sum_i [S_i \phi_{ri}^{1+\alpha} f_i^{1+\alpha}] \sum_i \phi_{ri} S_i} \quad (8)$$

As stated in Section “Estimation of Required Supplemental Damping”, the required damping ratio from the damper system,  $\xi_d$ , is 15%. When more than one ground motion is used for the analysis, the roof response amplitude,  $A$ , may be considered as the largest value of the maximum roof displacement response

under different ground motions obtained through time history analysis of the structure without FVDs but with the required effective damping ratio (Banazadeh, 2017). For the present study, the value of  $A$  is evaluated to be 0.3 m. Further, in the present study, the FVDs are considered to be implemented through diagonal braces. In such a case, the magnification factor,  $f_j$ , is equal to  $\cos \theta_j$ , where  $\theta_j$  is the angle between the horizontal and the brace that contains the FVD in the  $j^{th}$  story (Hwang et al., 2013). With these values of  $\xi_d$ ,  $A$  and  $f_j$ , the damping coefficient at each story as per Equation (8) is obtained and presented in the Table 4. As the damping coefficient obtained for the top story is quite less, it has not been considered in the designed damper scheme and hence, 11 FVDs are considered to be installed in the building (Figure 7).

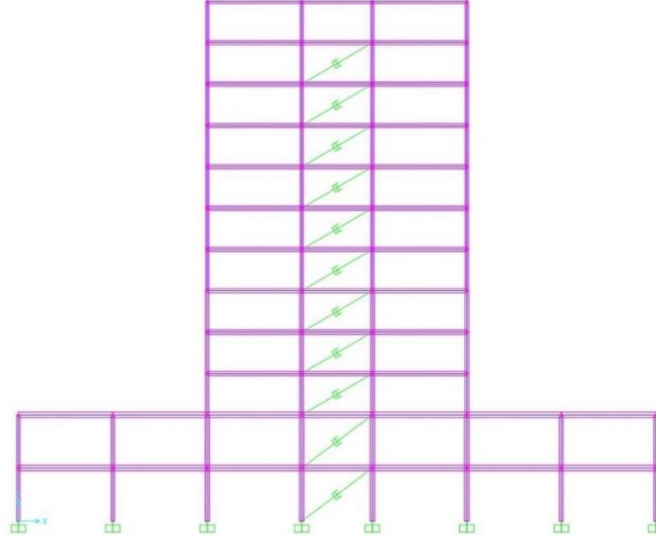


Fig. 7 Placement of the dampers

Next, it is of interest to design the stiffness of the brace that contains the FVD. It is established that brace flexibility affects the performance of the supporting FVDs (Lu et al., 2012). Several studies have been carried out to study the effect of brace stiffness,  $K$ , on the energy dissipation by the FVD and there is a wide variation in the suggested value of the optimum  $K$  that provides an adequate damper effect without requiring large sections of bracing elements (Singh et al., 2003; Londoño et al., 2014; Bruschi et al., 2022; Lavan, 2015). Given the disparity between different suggested values of optimum  $K$ , a study is carried out to find the optimal value of  $K$  for the present design. In this study, five values of  $K$  are considered, varying from fairly flexible to fairly stiff case.  $K$  is assumed to be proportional to the product of damping coefficient,  $C$ , and fundamental natural frequency,  $\omega$ . For each value of  $K$ , the frame is subjected to ground motions Input A and Input C. A remarkable increase is observed (Figure 8) in the roof displacement response reduction with increase in brace stiffness from  $K = 7C\omega$  to  $K = 13C\omega$  for both ground motions. For Input C, the roof displacement response reduction reduces with an increase in brace stiffness beyond  $K = 13C\omega$ . Thus, the optimum brace stiffness under Input C is  $13C\omega$ . However, for input A, a significant reduction in the roof displacement was observed for  $K = 13C\omega$ , though the optimum value of  $K$  is not yet reached. As Input C is the stronger ground motion, the optimum brace stiffness for the present study is considered as  $K = 13C\omega$ .

A particular FVD, which is located at story-6, is selected for a more detailed examination, and its hysteresis loops for different values of  $K$  are compared (Figure 9). Figure 9 indicates that the damper connected with a stiffer brace provides a fatter hysteresis loop. Further, the peak damper force is larger for a damper element with a larger  $K$ . Based on the results presented in Figures 8 and 9, a brace with a  $K$  equal to  $13C\omega$  is considered to be appropriate for the present structure. The provided brace stiffnesses are presented in Table 4.

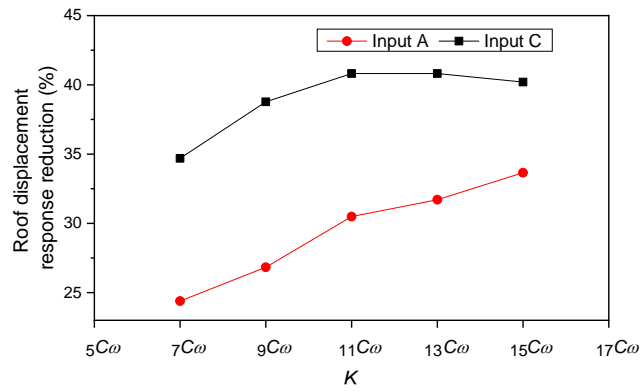


Fig. 8 Variation of roof displacement response reduction by FVD system with different brace stiffness,  $K$

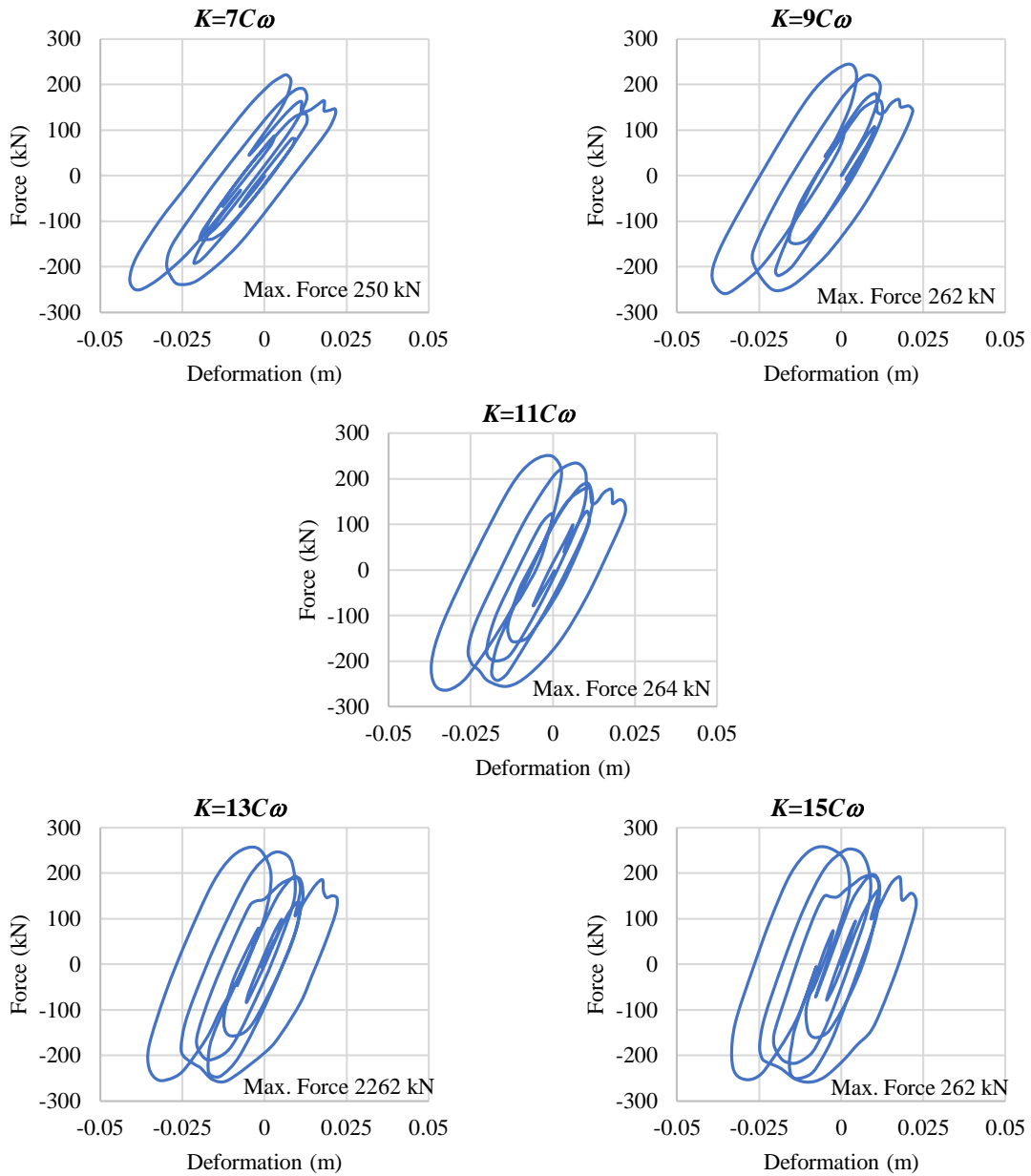


Fig. 9 Hysteresis loops of FVD located at story-6 for different brace stiffness,  $K$

**Table 4: Damping coefficients of FVDs and brace stiffness for different stories of the building**

Story	Damping Coefficient (C) (kN-s/m)	Brace Stiffness (K) (kN/m)
11	59.32	1796.64
10	157.56	4771.94
9	278.07	8421.46
8	373.41	11309.11
7	498.87	15108.72
6	579.63	17554.54
5	498.74	15104.73
4	533.53	16158.49
3	455.91	13807.80
2	287.97	8721.55
1	230.92	6993.53

For the nonlinear dynamic analysis in SAP2000 v20, FVDs are modeled as two-joint link elements, which have a nonlinear force-velocity relationship and are hence well suited for modeling FVDs. The link type is chosen as Damper Exponential. SAP2000 v20 uses the following nonlinear force-deformation relationship

$$f = C \operatorname{sgn}(v) |v|^\alpha \quad (9)$$

where  $C$  and  $\alpha$  are the damping coefficient and damping exponent of the FVD respectively.

In the SAP2000 v20 model, only one active degree of freedom, that is along the local axial direction (U1), is assigned for the damping elements.

## 2. Friction Damper (FD) System

In order to compare the two types of dampers, the distribution of the FDs is also made proportional to story shear strain energy, as in the case of the FVD scheme. An attempt is made to develop a preliminary formula for the distribution of slip loads of FDs proportional to story shear strain energy. Initially, the maximum forces in dampers at each story are determined based on the suggested distribution method. Then, an iterative study is carried out to obtain the appropriate slip load of each damper.

For an SDOF system, the relationship between the energy dissipated per cycle ( $E_d$ ), equivalent viscous damping ( $\zeta_d$ ), and maximum elastic strain energy ( $E_s$ ) is given as follows (Clough and Penzien, 2003).

$$\zeta_d = \frac{E_d}{4\pi E_s} \quad (10)$$

For an MDOF system, Equation (10) may be extended to Lin et al. (2000),

$$\xi_{dj} = \frac{E_d^j}{4\pi E_s^j} \quad (11)$$

where,  $\xi_{dj}$ ,  $E_d^j$ , and  $E_s^j$  denote equivalent viscous damping ratio, energy dissipated per cycle by the supplemental dampers, and maximum elastic strain energy of the structure with the supplemental dampers for the  $i^{th}$  mode of vibration.

Let the maximum force and maximum deformation in a FD be  $F_j$  and  $x$  respectively. For an ideal FD having a rectangular hysteresis loop,  $E_d^j$  can be written as

$$E_d^j = 4F_j|x| = 4F_j(\phi_j - \phi_{j-1}) \cos \theta_j \quad (12)$$

where,  $\cos \theta_j$  and  $\phi_j$  represent the damper configuration and the mode shape coefficient at the  $j^{th}$  story.

Further,  $E_s$  is equal to Hwang et al. (2013),

$$E_s = \frac{2\pi^2}{T^2} \sum_i m_i \phi_i^2 \quad (13)$$

Substituting Equations (12) and (13) in Equation (11) the following is obtained.

$$\xi_d = \frac{\sum_j 4F_j(\phi_j - \phi_{j-1}) \cos \theta_j}{4\pi \left( \frac{2\pi^2}{T^2} \sum_i m_i \phi_i^2 \right)} \quad (14)$$

Now, the maximum force in the damper proportional to strain energy can be expressed as

$$F_j = kS_j(\phi_j - \phi_{j-1}) = kS_j\phi_{rj} \tag{15}$$

where  $k$  is the proportionality constant.

The total damper force in the structure is then equal to

$$\sum_i F_i = k \sum_i S_i \phi_{ri} \tag{16}$$

From Equations (15) and (16),

$$F_j = \frac{S_j\phi_{rj}}{\sum_i S_i\phi_{ri}} \sum_i F_i \tag{17}$$

Substituting Equation (17) in Equation (14) and rearranging the terms, the following is obtained.

$$\sum_j F_j = \frac{\xi_d \cdot \frac{8\pi^3}{T^2} \sum m_i \phi_i^2}{\sum \frac{4S_j \phi_{rj}^2 f_j}{(\sum S_j \phi_{rj})}} \tag{18}$$

Again, on substituting Equation (18) in Equation (17), the maximum force in the damper at each story can be obtained as

$$F_j = \frac{2\pi^3 \cdot \xi_d (\sum m_i \phi_i^2) \cdot S_j \phi_{rj}}{T^2 f_j (\sum S_j \phi_{rj}^2)} \tag{19}$$

Thus, from Equation (19), a preliminary idea of the maximum damper force at each story can be obtained as per the approach of story shear strain energy proportional distribution.

Next, it is of interest to obtain the slip load at which each of the friction devices becomes operational. An iterative procedure is adopted to achieve this. Different trial values of slip loads are obtained by dividing the maximum force obtained from Equation (19) by different reduction factors. The corresponding reductions in roof displacement under Input A and Input C are obtained. The reduction factor versus roof displacement response reduction is plotted in Figure 10. It can be observed from Figure 10 that for Input A (moderate), the initial response reduction increases considerably with an increase in the reduction factor. However, smaller increments are noted at higher reduction factors. Further, with an increase in the reduction factor beyond 2.2, a localized fall in the response reduction is observed. For Input C (strong), there is not much variation in response reduction for the range of reduction factor from 1.5 to 2.4. However, for higher reduction factors, the damper effectiveness gradually reduces. Therefore, a reduction factor of 2.2 is selected as an appropriate value for the determination of the slip load of the FDs.

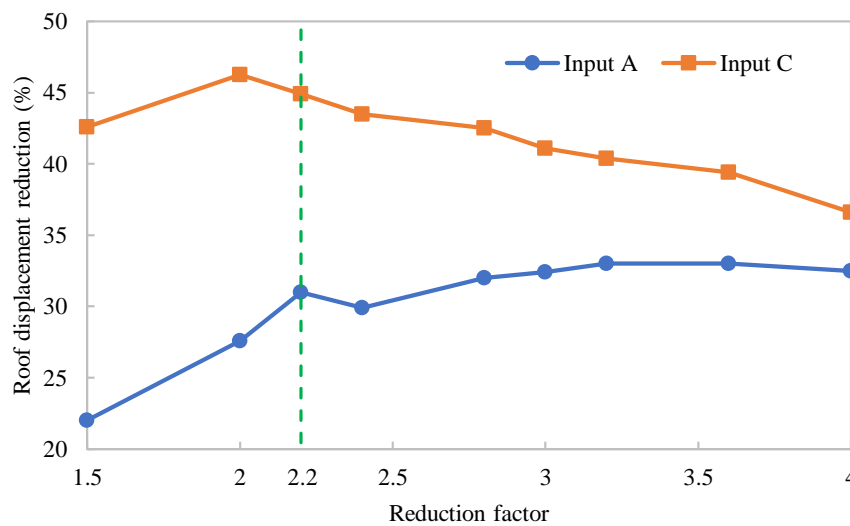


Fig. 10 Roof displacement response reduction vs. FD slip force reduction factor

As in the case of the FVD system (Figure 7), the FD system is also modeled as a damped brace system. Here, the damped brace should have yield strength equal to the slip load of the corresponding FD. In SAP2000 v20, the single diagonal tension/compression brace with friction damper is modeled as a damped

brace using the Plastic (Wen) type link. The following nonlinear force-deformation relationship of the damped brace is used by SAP2000 v20.

$$f = a \cdot K \cdot d + (1 - a) \cdot F_{slip} \cdot z \quad (20)$$

where  $K$ ,  $a$ ,  $d$ ,  $F_{slip}$ , and  $z$  respectively represent the initial elastic stiffness of the brace, the ratio of post-yield stiffness to elastic stiffness of the brace, the displacement, the slip load, and an internal hysteretic variable given by Equation (21).

$$\dot{z} = \frac{K}{F_{slip}} [\dot{d} (1 - |z|^{exp}), \text{ if } \dot{d}z > 0 \quad (21)$$

In Equation (21),  $exp$  is an exponent having a value greater than or equal to unity. Larger values of this exponent increase the sharpness of yielding. Equation (21) is a special case of the Bouc-Wen model (Wen, 1976).

As in the case of the FVD, only one active degree of freedom (U1) along the length of the bracing is specified for the FD. The brace stiffness is also specified to be the same as in the case of the FVD scheme to facilitate comparison. A yielding exponent of 10 is considered. Such a high value of yielding exponent permits a sharper transition from linear to nonlinear phase as compared to a lower yielding exponent value. As an FD slips at approximately constant load, the post-yield stiffness ratio can be estimated at near *zero*, therefore, in the present modeling, it is taken as 0.0001. Based on these parameters, the slip loads of the FDs are presented in Table 5.

**Table 5: Story-wise distribution of slip loads of FDs for example building**

Story	Slip Force (kN)
11	26.72
10	70.96
9	125.23
8	168.17
7	224.67
6	261.04
5	224.61
4	240.28
3	205.33
2	129.69
1	103.99

## NONLINEAR DYNAMIC ANALYSIS OF BUILDING WITH AND WITHOUT DAMPERS

To evaluate the performance of the building equipped with the two kinds of damper systems designed in Section “Design of Damper Systems”, nonlinear dynamic analysis is performed using SAP2000 v20 by subjecting the building to recorded base excitations as described in Table 3. The solution method adopted for analysis is the Direct-Integration method which solves the equations of motion without the use of modal superposition. For time history analysis, the default Hilber-Hughes-Taylor method with a time integration parameter equal to -0.1 is used.

From the modal analysis of the building with and without dampers, the natural periods of the first three modes of the building are determined and presented in Table 6. It is observed that the natural periods of the controlled building are reduced for all three modes. This is due to the additional stiffness contributed by the diagonal braces fitted with the dampers. This is often viewed as an advantage of the distributed damper systems, such as FVDs and FDs, that are integrated with the structural frame.

**Table 6: Modal periods example building**

Mode	Without dampers	With dampers
1	2.79 s	2.17 s
2	1.02 s	0.83 s
3	0.65 s	0.53 s

Table 7 presents the percentage reduction in peak floor displacements for the three considered ground motions. It may be observed that both damper systems provide a significant reduction in peak floor

displacements. Under Input A, the FVD system reduces the peak displacement of the lower floors more efficiently; while the reductions in peak displacement of the top three floors by both the damper systems are identical. A small increase in peak displacement of floors below the setback is noticed for ground motion Input B, but the magnitude of displacement is not significant at these lower floors. Under both Inputs B and C, the peak floor displacement reduction achieved by the FD system is almost the same as that of the FVD system for lower floors. However, for the 7<sup>th</sup> floor and above, the FD system clearly outperforms the FVD system so far as peak floor displacement response reduction is concerned. A set of indicative displacement time histories of the 12<sup>th</sup> floor (roof) of the controlled and uncontrolled building under Input A is plotted in Figure 11. Figure 12 depicts the variation of peak floor accelerations of the controlled and uncontrolled building structure for the considered ground motions. Both damper schemes have reduced the acceleration response to almost the same extent and with significant magnitude under Inputs A and C. However, the FVD system has a slight advantage over the FD, especially for the upper floors. Under Input B, there are also significant reductions in peak floor accelerations by both the damper systems; though the FVD system performs relatively better. Thus, the story shear strain energy-based distribution of dampers works well for the vertically irregular building and results in a significant reduction in both peak floor displacement and acceleration.

The hysteresis loops of the two kinds of devices from the third and eighth story of the building under ground motion Inputs B and C are presented in Figure 13, which indicates comparable energy dissipation by the dampers.

**Table 7: Percentage reduction in peak floor displacements under considered ground motions**

Floor	Input A		Input B		Input C	
	FVD	FD	FVD	FD	FVD	FD
1	28.05	15.78	-7.05	-6.72	18.44	16.16
2	30.39	19.57	-5.26	-5.66	19.18	17.44
3	30.16	19.60	2.80	2.07	24.91	24.49
4	29.74	19.47	13.18	13.15	16.87	22.12
5	29.17	19.47	20.41	21.50	16.85	17.69
6	29.74	21.28	28.18	30.72	20.75	15.91
7	34.79	27.84	32.58	36.08	17.08	18.87
8	37.88	32.22	34.06	38.05	21.02	23.40
9	38.55	35.40	34.34	38.74	28.43	30.80
10	37.74	36.94	33.98	38.93	36.05	38.22
11	36.33	36.11	33.70	39.11	40.35	42.74
12	35.92	35.76	33.60	39.12	41.21	43.66

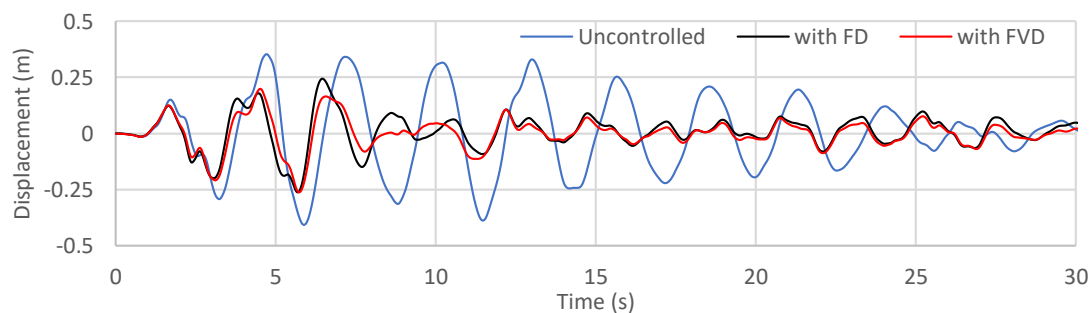


Fig. 11 Displacement time histories of the roof of controlled and uncontrolled building under Input A

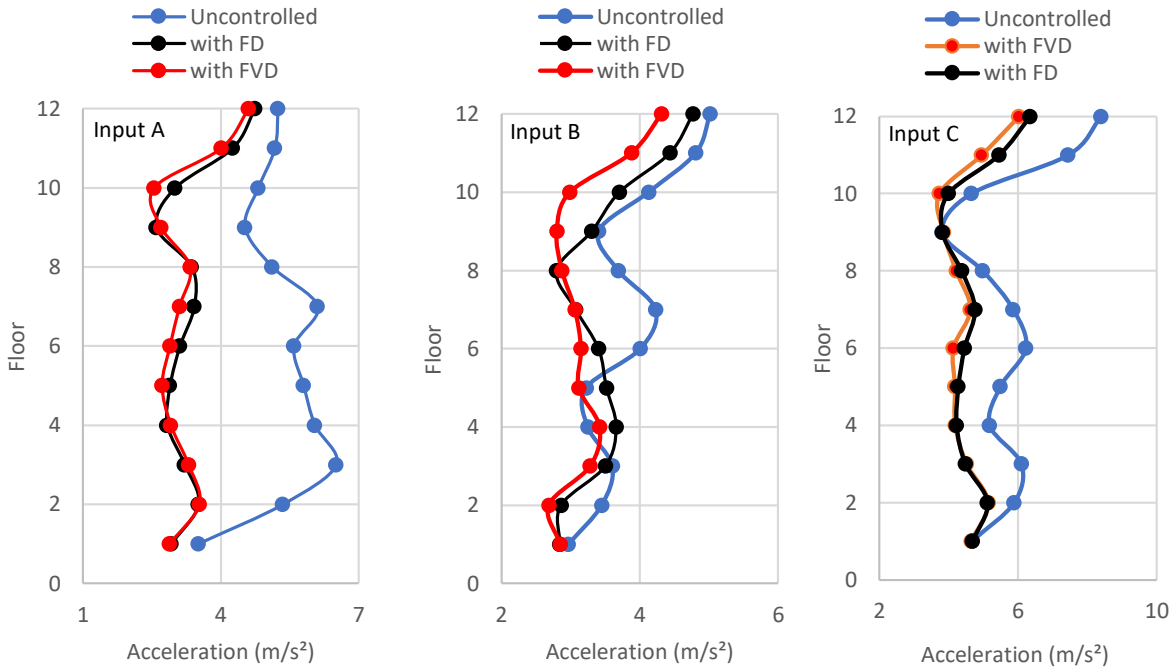


Fig. 12 Comparison of peak floor accelerations of controlled and uncontrolled building

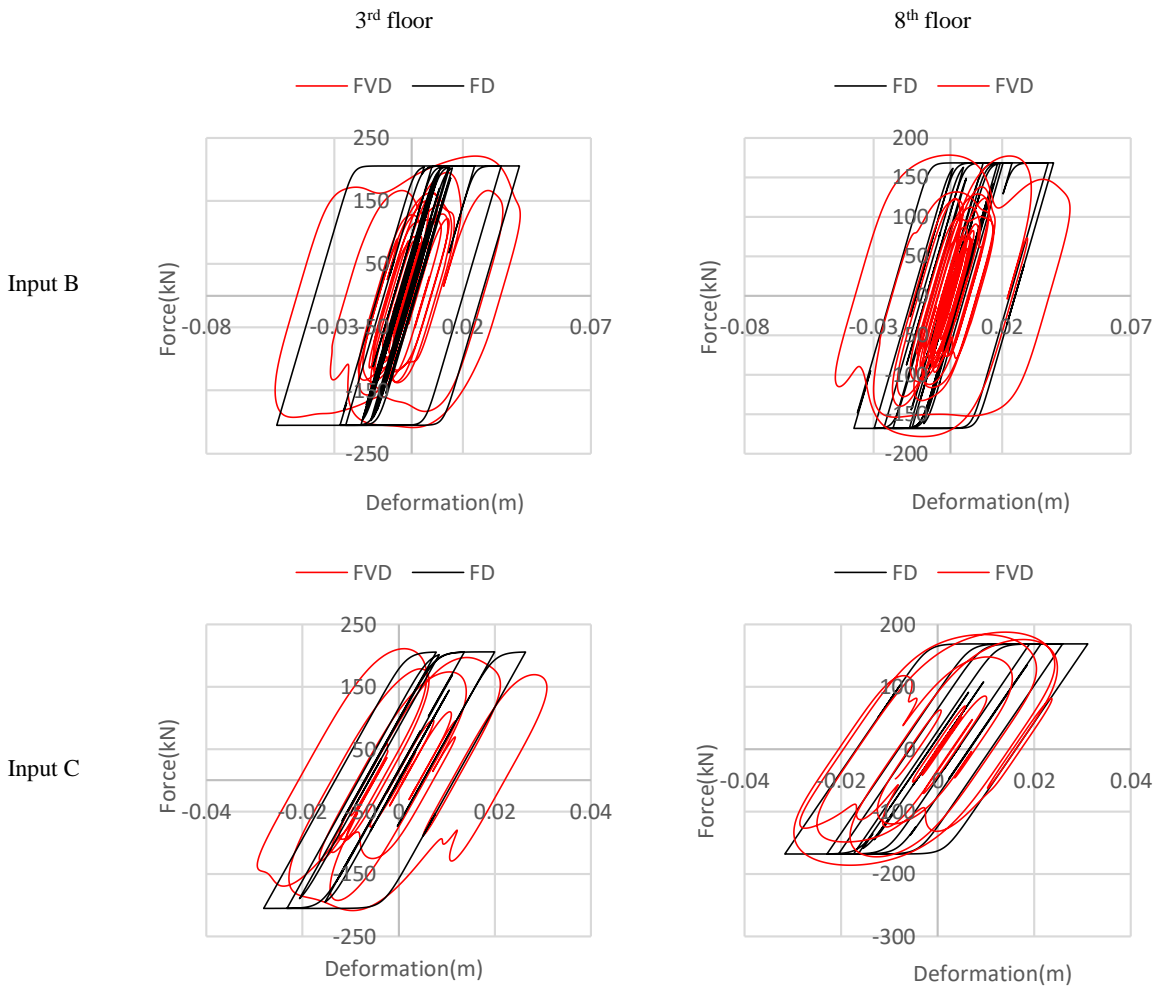


Fig. 13 Comparison of hysteresis loops of dampers

## CONCLUSIONS

Among the variety of supplemental devices, fluid viscous dampers (FVDs) and friction dampers (FDs) have gained popularity owing to their commercial availability. It would be interesting to know which of these devices would prove to be more beneficial under a given set of conditions. Vertical irregularities being a common feature in modern-day buildings, a steel building with vertical setbacks is considered for the present study. To compare the performance of the two devices, responses of the considered building fitted with FVDs and with FDs are investigated under recorded earthquake accelerograms. The Capacity Spectrum Method (CSM) is used to determine the amount of supplemental damping required to limit the maximum response of the structure to within the desired performance level. The approach of story shear strain energy proportional distribution of the dampers is followed. In case of the FVD scheme, an expression is formulated to distribute the damping coefficients of nonlinear FVDs along the height of the building. For FDs, the same approach is adopted to determine the maximum forces in dampers, which are further modified to obtain the slip loads through an iterative process. It is recognized from the literature that brace stiffness affects the performance of dampers. Therefore, a study to determine the optimal brace size for the given structure is accomplished. Again, to evaluate the performance of the damper devices based on the suggested distribution method, nonlinear dynamic analysis is performed using three considered input ground motions of varying intensity levels. The major inferences drawn from the entire work are presented below.

- i. The performance of dampers is found to be affected by the stiffness of brace containing dampers. With the increase in brace stiffness, hysteresis loops progressively become fatter for FVDs, and then assume a constant shape beyond a particular value of brace stiffness.
- ii. Under the considered ground motions, FVDs and FDs reduce the peak roof displacement by 34 to 41% and 36 to 44% respectively. Thus, both FVD and FD systems significantly reduce the displacement responses of the building. However, FDs achieve a larger reduction in the displacement response under strong ground motion (Input C). Under Input C, the reduction in the peak roof displacement by FDs and FVDs are 44% and 41% respectively.
- iii. The acceleration responses are also decreased for all the considered input ground motions. FVDs and FDs reduce the peak floor acceleration by 14 to 29% and 5 to 27% respectively. Comparatively, the FVD system performs better than the FD system under all the considered seismic inputs.
- iv. For the building with vertical setbacks, the design of both the FVD and FD systems, carried out by the story shear strain energy proportional distribution technique, works well in reducing the peak floor displacements and accelerations.

In the present study, nonlinear time history analysis was conducted for both the uncontrolled and controlled structures under input base ground motions. The performance of the dampers is represented in terms of the reductions in structural response, namely the peak floor displacement and peak floor acceleration. The assessment of whether the dampers are able to bring the response within the desired point on the capacity spectrum determined during the damper design will be considered as a future scope of work.

## REFERENCES

1. Ahmed, M.M.M., Abdo, M.A.B. and Mohamed, W.A.E.W. (2022). "Vertical Geometric Irregularity Effect on Performance-Based Seismic Design for Moderate Rise RC Moment Resisting Frame Buildings", *Arabian Journal for Science and Engineering*, Vol. 47, pp. 12333–48.
2. ATC 40 Vol 1. (1996). "Seismic Evaluation and Retrofit of Concrete Buildings", *Applied Technology Council*, California, USA.
3. Banazadeh, M., Ghanbari, A. and Ghanbari, R. (2017). "Seismic Performance Assessment of Steel Moment-Resisting Frames Equipped with Linear and Nonlinear Fluid Viscous Dampers with the Same Damping Ratio", *Journal of Constructional Steel Research*, Elsevier, Vol. 136, pp. 215–28.
4. Bruschi, E., Quaglini, V. and Calvi, P.M. (2022). "A Simplified Design Procedure for Seismic Upgrade of Frame Structures Equipped with Hysteretic Dampers", *Engineering Structures*, Vol. 251, pp. 113504.

5. Clough, R.W. and Penzien, J. (2003). "Dynamics of Structures", 3<sup>rd</sup>, Editor. *Computers & Structures, Inc.*, Berkeley, USA.
6. Damptech (2021). "12 Projects in Japan using Damptech Dampers", Retrieved from <https://www.damptech.com/japan> (Accessed December 12, 2023).
7. De Domenico, D., Ricciardi, G. and Takewaki, I. (2019). "Design Strategies of Viscous Dampers for Seismic Protection of Building Structures: A Review", *Soil Dynamics and Earthquake Engineering*, Vol. 118, pp. 144–65.
8. de Silva, C.W. (1981). "An Algorithm for the Optimal Design of Passive Vibration Controllers for Flexible Systems", *Journal of Sound and Vibration*, Vol. 75, pp. 495–502.
9. FEMA 356. (2000). "Prestandard and Commentary for the Seismic Rehabilitation of Buildings", *Fed. Emerg. Manag. Agency*, Washington, D.C, USA.
10. Ferraioli, M., Lavino, A. and Mandara, A. (2016). "An Adaptive Capacity Spectrum Method for Estimating Seismic Response of Steel Moment-Resisting Frames", *Ingegneria Sismica*, Vol. 33, pp. 47–60.
11. Freeman, S.A. (2004). "Review of the Development of the Capacity Spectrum Method", *ASET Journal of Earthquake Technology*, Vol. 41, pp. 113.
12. Ghosh, A.D. and Konar, T. (2023). "Popular Passive Dampers for Structural Control: A Review", *Journal of Structural Engineering (Madras)*, Vol. 50, pp. 24–38.
13. Hanson, R. and Soong, T. (2001). "Seismic Design with Supplemental Energy Dissipation Devices", *Earthquake Engineering Research Institute*, Oakland, CA, USA.
14. Housner, G.W., Bergman, L.A., Caughey, T.K., Chassiakos, A.G., Claus, R.O. and Masri, S.F. (1997). "Structural Control: Past, Present, and Future", *Journal of Engineering Mechanics*, Vol. 123, pp. 897–971.
15. Hwang, J., Lin, W. and Wu, N. (2013). "Comparison of Distribution Methods for Viscous Damping Coefficients to Buildings", *Structure and Infrastructure Engineering*, Vol. 9, pp. 28–41.
16. IS:1893 (Part-1). (2016). "Criteria for Earthquake Resistant Design of Structures : General Provisions and Buildings", *Bureau of Indian Standards*, New Delhi.
17. Jaisee, S., Yue, F. and Ooi, Y.H. (2021). "A State-of-the-Art Review on Passive Friction Dampers and their Applications", *Engineering Structures*, Vol. 235.
18. Kareem, A., Kijewski, T. and Tamura, Y. (1999). "Mitigation of Motions of Tall Buildings with Specific Examples of Recent Applications", *Wind and Structures*, Vol. 2, pp. 201–51.
19. Lago, A., Faridani, H.M. and Trabucco, D. (2018). "Tall Buildings in Numbers-World's Tallest Buildings with Dampers", *CTBUH Journal*, pp. 48–9.
20. Lavan, O. (2015). "Optimal Design of Viscous Dampers and Their Supporting Members for the Seismic Retrofitting of 3D Irregular Frame Structures", *Journal OfStructural Engineering*, Vol. 141, pp. 04015026.
21. Lin, X., Moss, P.J. and Carr, A.J. (2000). "Seismic Analysis and Design of Building Structures with Supplemental Lead Dampers", *12<sup>th</sup> World Conference on Earthquake Engineering*, Auckland, New Zealand. pp. 1417.
22. Londoño, J.M., Wagg, D.J. and Neild, S.A. (2014). "Supporting Brace Sizing in Structures with Added Linear Viscous Fluid Dampers: A Filter Design Solution", *Earthquake Engineering and Structural Dynamics*, Vol. 43, pp. 1999–2013.
23. Lu, Y.X., Cai, Y.Q., Qu, Q.F. and Zhan, Q.H. (2012). "Study on the Effect of Supporting Stiffness on Energy Dissipation Efficiency of Viscous Dampers", *Applied Mechanics and Materials*, Vol. 105–107, pp. 96–101.
24. Mouhine, M. and Hilali, E. (2022). "Seismic Vulnerability Assessment of RC Buildings with Setback Irregularity", *Ain Shams Engineering Journal*, Vol. 13, pp. 101486.
25. Moustafa, A. (2011). "Damage-Based Design Earthquake Loads for Single-Degree-Of-Freedom Inelastic Structures", *Journal of Structural Engineering*, Vol. 137, pp. 456–67.
26. Narkhede, D.I. and Sinha, R. (1999). "Shock Vibration Control of Structures using Fluid Viscous Dampers", *15<sup>th</sup> World Conference on Earthquake Engineering*, Lisbon, Portugal.

27. Pall, A.S. and Pall, R.T. (2004). "Performance-Based Design Using Pall Friction Dampers - an Economical Design Solution", *13<sup>th</sup> World Conference on Earthquake Engineering*, Vancouver, Canada. pp. 1955.
28. Pall, A.S., Marsh, C. and Fazio, P. (1980). "Friction Joints for Seismic Control of Large Panel Structures", *Journal - Prestressed Concrete Institute*, Vol. 25, pp. 38–61.
29. Pall Dynamics (n.d.). "Seismic Upgrade of Boeing Commercial Airplane Factory", Retrieved from [https://www.palldynamics.com/P1\\_usa.htm](https://www.palldynamics.com/P1_usa.htm) (Accessed December 12, 2023).
30. PEER. (n.d.). "PEER Ground Motion Database -Pacific Earthquake Engineering Research Center", Internet (Accessed December 12, 2023).
31. Qian, F., Ding, S., Song, J. and Chen, C.-C. (2012). "Testing of Fluid Viscous Damper", *15<sup>th</sup> World Conference on Earthquake Engineering (15WCEE)*, Lisbon, Portugal.
32. Quaketek (2020). "Featured Applications", Retrieved from <https://quaketek.com/applications/> (Accessed December 12, 2023).
33. Rodgers, J.E. and Mahin, S.A. (2004). "Effects of Connection Hysteretic Degradation on the Seismic Behavior of Steel Moment-Resisting Frames", *Pacific Earthquake Engineering Research Center*.
34. Sarkar, P., Prasad, A.M. and Menon, D. (2010). "Vertical Geometric Irregularity in Stepped Building Frames", *Engineering Structures*, Vol. 32, pp. 2175–82.
35. Seleemah, A.A. and Constantinou, M.C. (1997). "Investigation of Seismic Response of Buildings with Linear and Nonlinear Fluid Viscous Dampers", *Tech. Rep. NCEER-97-0004*. Buffalo, New York, USA.
36. Shah, A.H., Sharma, U.K., Kamath, P., Bhargava, P., Reddy, G.R. and Singh, T. (2016). "Effect of Ductile Detailing on the Performance of a Reinforced Concrete Building Frame Subjected to Earthquake and Fire", *Journal of Performance of Constructed Facilities*, Vol. 30, pp. 1–17.
37. Singh, M.P., Verma, N.P. and Moreschi, L.M. (2003). "Seismic Analysis and Design with Maxwell Dampers", *Journal of Engineering Mechanics*, Vol. 129, pp. 273–82.
38. Taiyari, F., Mazzolani, F.M. and Bagheri, S. (2019). "Damage-Based Optimal Design of Friction Dampers in Multistory Chevron Braced Steel Frames", *Soil Dynamics and Earthquake Engineering*, Vol. 119, pp. 11–20.
39. Ucar, T. and Merter, O. (2019). "Effect of Design Spectral Shape on Inelastic Response of RC Frames Subjected to Spectrum Matched Ground Motions", *Structural Engineering and Mechanics*, Vol. 69, pp. 293–306.
40. Wen, Y.K. (1976). "Method for Random Vibration of Hysteretic Systems", *ASCE J Eng Mech Div*, Vol. 102, pp. 249–63.